

Assessment of the modulation effect of rainfall on solar radiation availability at the Earth's surface

J. J. Díaz-Torres,^{a*} L. Hernández-Mena,^a M. A. Murillo-Tovar,^{b,c} E. León-Becerril,^a A. López-López,^a C. Suárez-Plascencia,^d E. Aviña-Rodríguez,^d A. Barradas-Giméte^e and V. Ojeda-Castillo^e

^a Department of Environmental Technology, Center for Research and Assistance in Technology and Design of the State of Jalisco, Guadalajara, Mexico

^b National Council for Science and Technology, Cátedras Program, Mexico City, Mexico

^c Chemical Research Center, Autonomous University of the Morelos State, Cuernavaca, Mexico

^d Department of Geography and Spatial Planning, University of Guadalajara, Mexico

^e Interinstitutional Postgraduate in Science and Technology, Center for Research and Assistance in Technology and Design of the State of Jalisco, Mexico

ABSTRACT: A significant proportion of the solar irradiance that reaches the Earth's surface is normally attenuated by atmospheric properties and overcast conditions related to the rainy season. The Solar Analyst (SA) model, irradiance and long term precipitation data were used to assess this relationship in Guadalajara, Mexico. A spatial analysis based on morphological and statistical criteria increased the model's certainty. The SA model explains 95.4% of the irradiation variability observed on the ground, with average uncertainties of 3.7% during clear sky conditions in the dry season and 4.4% on sunny days in the wet season. The meteorological data analysis shows that total precipitation in 2014 had an atypical temporal distribution and was slightly lower (12.6%) than the average from 1991 to 2012. A deficit of 39% in precipitation compared to the long term average was found in the first half of the season, which was later partially compensated. This deficit was interpreted as a temporary delay in high values of precipitation. Based on the potential average irradiation from the SA model and field observations, it can be concluded that overcast conditions related to rainfall through 2014 attenuated approximately 28.5% of the incoming solar energy. Taking the global energy balance into account, this fraction was higher in comparison to the energy proportion reflected by the cloud's albedo (*ca* 23%). These results suggest that both the high proportion of energy attenuated and atypical weather conditions may be local effects of large-scale phenomena such as the El Niño-Southern Oscillation.

KEY WORDS irradiation; rainfall; overcast conditions; Solar Analyst; ENSO; Guadalajara

Received 8 March 2016; Revised 15 July 2016; Accepted 20 July 2016

1. Introduction

Solar energy has direct effects on many physical, chemical and biological cycles (Fu and Rich, 1999; Finlayson-Pitts and Pitts, 2000; Fu, 2003). The irradiance and rainfall are key factors in understanding climate variability. These two variables largely determine the weather of a region, and may lead to the formation of pollutant compounds in the atmosphere by photochemical processes derived from chemical precursors (Finlayson-Pitts and Pitts, 2000). Consequently, a substantial proportion of radiant energy is attenuated in different ways (due to smog, haze or fog) (Jauregui and Luyando, 1999; Elias *et al.*, 2009). The relationship between the irradiance and rainfall also reflects the behaviour of large-scale phenomena such as the El Niño-Southern Oscillation (ENSO), which has the ability to modify the normal conditions of the atmosphere in many regions of the planet, altering local weather patterns. Therefore, solar irradiation and its influence upon the climate has been addressed through different perspectives and methodological approaches, based mainly on

the energy balance and transfer mechanisms between the oceans, atmosphere and land masses (Lewis *et al.*, 1990; Kiehl and Trenberth, 1997; Trenberth *et al.*, 2009).

In order to estimate solar irradiation, some methods consider the topography and atmospheric components as the main factors under investigation (Garnier and Ohmura, 1968; Williams *et al.*, 1972; Swift, 1976; Revfeim, 1978). Others have estimated radiation indirectly by calculation of meteorological variable parameters (Reddy, 1971, 1974; Atwater and Brown, 1974; Atwater and Ball, 1978); meanwhile, further studies have implemented algorithms to estimate the incidence of solar radiation at the surface by using satellite images (Tarpyley, 1979; Pinker and Laszlo, 1992; Noia *et al.*, 1993a, 1993b; Perez *et al.*, 2002, 2009). Some of the last-mentioned methodologies have provided important approaches to the estimation and forecasting of the amount of radiation in the synoptic scale domain (e.g. data from the National Renewable Energy Laboratory (NREL) and the National Aeronautics and Space Administration (NASA)) (<http://maps.nrel.gov/swera/>). However, their spatial resolution (*ca* 20 and 60 arcmin, respectively) prevents the identification of significant variations of radiation on smaller surfaces (Tovar-Pescador *et al.*, 2006; Ruiz-Arias *et al.*, 2009).

Artificial neural network techniques have been proposed as a reliable method for the calculation of daily solar radiation. A high level of confidence in global solar radiation predictions can

* Correspondence: J. J. Díaz-Torres, Department of Environmental Technology, Center for Research and Assistance in Technology and Design of the State of Jalisco, 800 Normalistas Ave, Guadalajara, Jalisco, Mexico. E-mail: jdiaz@ciatej.mx

be reached with this method, both in time and space (Bosch *et al.*, 2008; Behrang *et al.*, 2010; Şenkal, 2010; Koca *et al.*, 2011; Linares-Rodríguez *et al.*, 2011). The artificial neural networks method is based on a training process which involves mainly the use of data from a weather monitoring network, satellite images, digital elevation models and time series with several years of records. Moreover, models coupled to computer systems such as geographic information systems (GISs) have been developed. These models are independent of meteorological data availability and an homogeneous monitoring network. Among them are the following: SolarFlux (Solar Analyst, SA) designed on the ARC/INFO platform (Herrick *et al.*, 1993; Dubayah and Rich, 1995), the Soleil Model linked to IDRISI (Miklának, 1993), Genasys (Kumar *et al.*, 1997), SRAD (McKenney *et al.*, 1999; Wilson and Gallant, 2000), r.sun adapted to the GRASS environment (Hofierka and Suri, 2002), Miramon GIS (Pons, 2002; Pons and Ninyerola, 2008) and the development of some algorithms proposed on their own (Zakšek *et al.*, 2005).

Recently, the SA, r.sun, Solei-32 and SRAD models were evaluated on the same surface. The study compared the response of these models to determine their effectiveness (Ruiz-Arias *et al.*, 2009). Some differences were shown between the models, highlighting the way in which every model determines the attenuating capacity of the atmosphere. On a daily temporal scale, all models except SRAD had good correlation regarding field observations in the study area, with a determination co-efficient (R^2) between 91 and 94%. The r.sun and Solei-32 models proved the best fit to the field observations, allowing the use of parameters such as Linke's turbidity and the Rayleigh effect to correct the model estimations whilst they were running (Ruiz-Arias *et al.*, 2009). Nonetheless, in the case of the SA model, the field observations helped to find the transmittance and diffusion parameters to characterize the state of the atmosphere later for some model tests. The SA model has proven to be an efficient and simple system for calculating the monthly solar irradiation (Herrick *et al.*, 1993; Dubayah and Rich, 1995; Fu and Rich, 1999), in both tropical and temperate regions and with complex topography (Rich *et al.*, 1993, 1994; Fu and Rich, 2002).

The GIS based models have been widely used to evaluate regional photovoltaic potential (Sorensen, 2001; Gastli and Charabi, 2010; Janke, 2010; Djurdjevic, 2011; Rumbayan *et al.*, 2012; Lee *et al.*, 2014), bioclimatic conditions (Rich *et al.*, 1992, 1993; Fu and Rich, 2002) and the effects of urban morphology on the availability of sunlight (Robinson and Stone, 2004; Robinson, 2006; Li and Wong, 2007; Yu *et al.*, 2009), among other important applications.

In Mexico and particularly in the Guadalajara Metropolitan Area (GMA), continuous and systematic monitoring of solar radiation is recent (Valdés-Barrón *et al.*, 2014); spatial and temporal distribution has barely been studied. There are studies that have exposed the behaviour of irradiation throughout the country (Almanza and Lopez, 1978; Galindo *et al.*, 1991; Campos-Aranda, 1992; Estrada-Cajigal and Almanza, 2005), whereas others have usually associated radiation with the behaviour of meteorological variables and pollutant concentrations in the GMA (Tereshchenko and Filonov, 1997; Davydova and Skiba, 1999; Ramírez-Sánchez *et al.*, 2009; Limón-Sánchez *et al.*, 2011).

At present, no research that precisely explains the relationship between irradiance and rainfall in the GMA is available. The present study evaluates the attenuating effect produced by the rainfall conditions upon the solar irradiation. Based on field information, the SA model was tested to characterize solar irradiation in a place where a widely monitoring network was not available

and disaggregated data for every component of the solar radiation were not registered. A spatial analysis on surfaces with similar topographical features was proposed to increase the certainty of the model. The methodology provides arguments to identify the irradiation–rainfall relationship at a local scale in the ENSO context.

The paper includes a section with the study area and solar irradiation overview. In the methodology, the quality of the data sources, model procedures, restrictions and limiting conditions, as well as the spatial and statistical analysis, are explained. In the results and discussion section, the rainfall analysis and the efficiency of the model response lead to estimates of the proportion of solar irradiation attenuated during the wet season. Finally, some conclusions on energy proportions and the relationship with the ENSO are made.

2. Study area and overview of solar radiation

2.1. The Guadalajara Metropolitan Area

Guadalajara is located in western Mexico ($20^{\circ} 39' 55''$ N, $103^{\circ} 20' 56''$ W), seated on a plain. Here, the Atemajac, Tesistán and Toluquilla valleys have developed, which are topographically delimited by volcanic structures such as La Primavera volcanic complex (LPVC), the volcanic range of southern Guadalajara (VRSG) and the Santiago River canyon (SRC) (Figure 1).

The predominant GMA surface elevations range between 1500 and 1675 m with elevations of 1585 m on average. The altitude of the ranges in the area reaches up to 2260 m, while the deep surface of the SRC reaches altitudes of 900 m near the study area. The GMA morphology is dominated by undulations with slopes of $<15^{\circ}$. Hillsides with slopes up to 30° are developed on the more prominent structures, while at the SRC surfaces slopes ranging from 15° to 45° predominate, although in some areas sloping cliffs protrude up to 80° .

The climate in the GMA region is warm and humid with summer rainfall (May–October) (García, 1988). According to the analysis of meteorological data for the period 1960–1996, the annual rainfall around Guadalajara was approximately 892.2 mm on average, with variations within the range 700–900 mm. The annual average temperature range is around 19.2°C (minimum 11.9°C , maximum 26.5°C) (Davydova and Skiba, 1999). In the dry season, stable atmospheric conditions occur with domination of an anti-cyclonic circulation, normally manifested by calm conditions and clear skies (Tereshchenko and Filonov, 1997; Davydova and Skiba, 1999).

2.2. Attenuation factors

Irradiance is defined as the amount of energy *per* unit area and *per* unit time (W m^{-2}) (instantaneous energy), while irradiation indicates the amount of solar energy *per* unit area accumulated at a specific time (Wh m^{-2}) (Hofierka and Suri, 2002). Under normal conditions at the top of the atmosphere, irradiance is $1367 \pm 3 \text{ W m}^{-2}$; this value was established as the solar constant (I_{SC}) by the World Radiation Center. Since the land surface is partially illuminated for an instant, it is estimated that the Earth receives on average 341 W m^{-2} (a quarter of I_{SC}). The Earth–atmosphere system reflects approximately 30% of the solar radiation depending on the surface, cloud cover and aerosol burden (Trenberth *et al.*, 2009). It is known that there is an average irradiance of 239 W m^{-2} , which is equivalent to a mean irradiation of $5.7 \text{ kWh m}^{-2} \text{ day}^{-1}$.

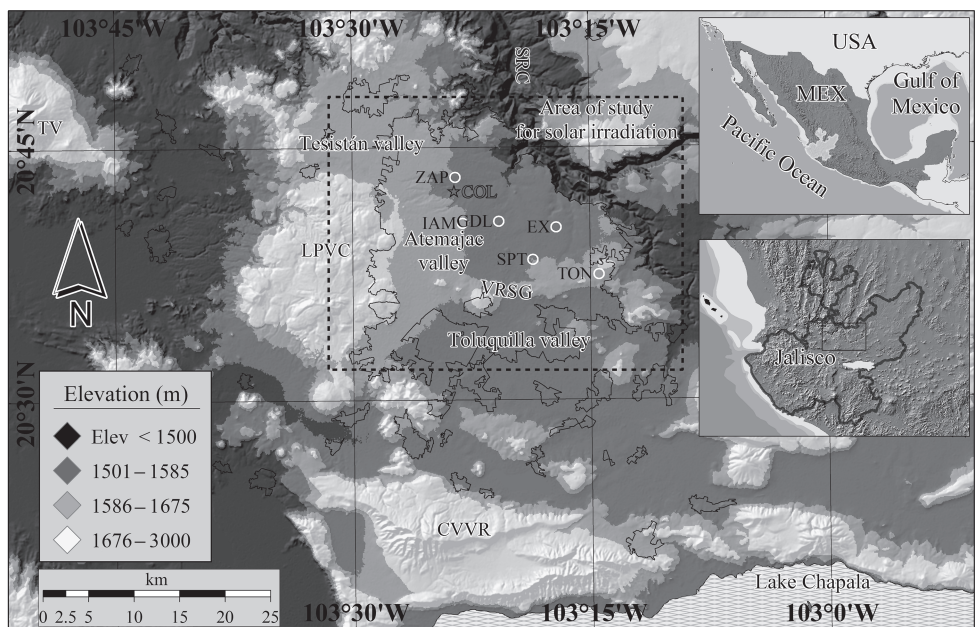


Figure 1. Study area location and its geographical environment. The area enclosed within the dotted line shows the effective surface in which the irradiation analysis was conducted. Irregular polygons correspond to the urban area of the Guadalajara Metropolitan Area. Location of the Colomos weather station, star; white outline circles indicate the position of the stations with historical data (1991–2012): Zapopan (ZAP); Guadalajara (GDL); San Pedro Tlaquepaque (SPT); Experience (EX); Tonalá (TON). VRSG, volcanic range of southern of Guadalajara; LPVC, La Primavera volcanic complex; RVVC, Cerro Viejo volcanic range; TV, Tequila Volcano; SRC, Santiago River Canyon.

The solar radiation at the surface is controlled by the attenuating effects of astronomical relations, the topographic properties and atmospheric conditions. In the case of astronomical relations some factors are implicated in the apparent Sun path (solar ecliptic), which involves factors such as distance and position of the Earth relative to the Sun for any day. Further, a set of geometric parameters is normally considered, including the solar declination angle (δ), the solar elevation angle (α), the zenith angle (θ) and the solar azimuth angle (ψ). These parameters are fundamental for calculating the magnitude of solar radiation incident on a surface and its changes through the annual cycle (Iqbal, 1983). Concerning the topography, the slope and surface orientation together with the topographic shadow effect are terrain properties that contribute to the solar radiation attenuation (Fu and Rich, 1999). These factors have been widely used in solar calculations (Garnier and Ohmura, 1968; Williams *et al.*, 1972; Swift and Knoerr, 1973; Revfeim, 1978; Burrough, 1986; Hofierka and Suri, 2002; Pons and Ninyerola, 2008).

On the other hand, the atmosphere is an anisotropic medium where the incident radiation varies according to the direction of propagation. In addition, the clouds are another attenuating factor with unpredictable behaviour. Although empirical techniques have been used to estimate their attenuating capability (Remund *et al.*, 2003; Ruiz-Arias *et al.*, 2009), there are still serious difficulties involved in the determination of their impact on the reduction of solar radiation. Hence, attenuation by atmospheric factors can only be modelled with a given level of accuracy (Hofierka and Suri, 2002; Ruiz-Arias *et al.*, 2009).

Transmittance and diffusion are two important atmospheric properties that reduce the proportion of radiation at the surface. Transmittance indicates the capacity of absorption and scattering of atmospheric components. Moreover, it acts as a filter that reduces a significant proportion of the radiant energy (Finlayson-Pitts and Pitts, 2000). The scattering of radiation depends on the optical air mass thickness (Fu and Rich, 1999).

This phenomenon involves two main dispersion mechanisms related to atmospheric gases: Mie and Rayleigh scattering. Both characterize a clear and dry atmosphere (Hofierka and Suri, 2002), which is composed almost entirely of gas molecules (e.g. oxygen and molecular nitrogen) (Finlayson-Pitts and Pitts, 2000; Monteith and Unsworth, 2013). Moreover, the turbidity attenuation is caused by the presence of water vapour and particulate matter. The presence of these components explains the optical density of the air and determines the diffusion effect (Hofierka and Suri, 2002).

3. Data and methodology

3.1. Digital elevation data and meteorological information

The digital elevation model (DEM) represents an essential resource to calculate the solar radiation, since it reproduces the effect of the mitigating factors previously mentioned (Herrick *et al.*, 1993; Dubayah and Rich, 1995). The radiation analysis was carried out using the 1 arcsec Shuttle Radar Topography Mission (SRTM) database from the EarthExplorer site. Descriptive statistics indicate that the DEM is free of artefacts (cells with values negative or equal to zero). These natural effects were discarded from the certainty calculation of the solar analysis. The histogram analysis shows that shallow and undulating surfaces were distributed mainly over a range of elevations from 1500 to 1675 m, corresponding to approximately 73.4% of the total area. Surfaces below 1500 m correspond to SRC relief (13.5%), and above 1675 m represent the protruding relief (13.1%) of the surrounding mountains (Figure 1).

The SA model validation was supported on the Colomos station, and was managed by the National Meteorological Survey in Mexico (NMS) (<http://smn.cna.gob.mx/es/emas>). The station was the only meteorological data source available in the study area for 2014. It shows average or cumulative values for a set of

variables, among them solar radiance, precipitation or temperature. The station records meteorological data every 60 s, 60 min and 24 h. Hourly and daily data were considered together to evaluate the model response. Meanwhile, the typical (climatic) behaviour of the rainfall was characterized by observations of rain accumulated over 24 h. These records were taken from five stations installed in the GMA by the Mexican Water Commission (Figure 1). The analysis was carried out during a period of 22 years (1991–2012).

3.2. The Solar Analyst model

Both the monthly and daily solar irradiation was calculated through the SA model with the methodology described by Fu and Rich (1999). The SA model integrates the three main attenuating factors of solar radiation; it is a system that was designed to calculate the potential global irradiation on surfaces with cloudless conditions. This model makes a segmented analysis of the DEM to calculate the Sun's apparent path, the incidence angle of radiation for a moment, the time of sunrise and sunset, and the time of the solar radiation exposure (Hetrick *et al.*, 1993; Dubayah and Rich, 1995).

The SA model assumes an isotropic state of the atmosphere and reproduces the atmospheric effect through diffusion and transmissivity co-efficients. It defines its effects through an inverse relationship whereby atmospheric transmittance decreases as atmospheric turbidity increases (Hetrick *et al.*, 1993; Dubayah and Rich, 1995). Because the atmospheric transmittance is closely related to relief, the model takes into account the topographic properties to calculate the air mass thickness of the atmosphere (Hetrick *et al.*, 1993).

Before integrating the global irradiation for a time period, the model calculates the instantaneous direct radiation ($I_{DR(\theta,\psi)}$) and the instantaneous diffuse radiation ($I_{DF(\theta,\psi)}$) based on the following equations (Hetrick *et al.*, 1993; Dubayah and Rich, 1995):

$$I_{DR(\theta,\psi)} = I_{SC} \cdot \tau^m \cdot \cos i \quad (1)$$

$$m = \frac{1}{\cos \theta} \quad (2)$$

$$I_{DF(\theta,\psi)} = I_{SC} \tau_d \cos^2 \left(\frac{\theta}{2} \right) \sin \alpha \quad (3)$$

$$\tau_d = 0.271 - (0.294 \tau^m) \quad (4)$$

The instantaneous direct radiation is referred to a sun position defined by zenith angle (θ) and azimuth angle (ψ). It is calculated based on the solar constant (I_{SC}), the transmissivity co-efficient (τ), the optical air mass (m) as a transmittance correction co-efficient (the last two vary depending on the time of day) and the angle formed between the Sun's rays' vector of incidence and the normal vector to the surface intercept (i) (Equations (1) and (2)). Meanwhile, the instantaneous diffuse radiation ($I_{DF(\theta,\psi)}$) (Equation (3)) takes into account the solar elevation (α), the slope (S) and a diffusion co-efficient (τ_d) which simulates the atmospheric turbidity (Equation (4)) (Hetrick *et al.*, 1993). The SA model is complemented by the standard overcast sky model that enhances the ability to calculate the diffuse radiation proportion on a surface depending upon the variation of θ (Hetrick *et al.*, 1993; Dubayah and Rich, 1995; Fu and Rich, 1999).

The SA model determines the potential global irradiation (I_G) by the hemispherical viewshed algorithm (Equation (5)). This algorithm solves the three attenuating factors of irradiation by adding the two main components of total solar radiation: direct (I_{DRT}) and diffuse (I_{DFT}) (Equations (6) and (7)). Irradiance coming from all possible directions for each DEM cell is integrated during a period of time (Rich *et al.*, 1994; Fu and Rich, 1999):

$$I_G = I_{DRT} + I_{DFT} \quad (5)$$

$$I_{DRT} = \sum I_{DR(\theta,\psi)} \quad (6)$$

$$I_{DFT} = \sum I_{DF(\theta,\psi)} \quad (7)$$

Ultimately, the model was executed to calculate the global irradiation, and each model response was integrated in the matrix array (surface).

3.3. Parameter settings

The SA model analysis was performed over the study area (Figure 1). The parameters proposed by Fu and Rich (1999) (Table 1) were taken as a reference, in order to identify the model response to explain the irradiation on the GMA. Several runs of the model were completed (Table 2), taking as a starting point a fraction of τ_d and τ from the same authors' suggestions (0.3 and 0.5, respectively). For this study, the field observations were taken from Colomos station, the only station measuring solar

Table 1. Parameters used to calculate irradiation through the Solar Analyst model.

Parameter	Value	Observations and references
Viewshed basin determination	24	Prominent terrain: 32 divisions. Flat surfaces: 8–16 divisions
Time interval in hours (sky sectors in sunmap)	0.5	Time period from which irradiation is calculated (hours). 0.5 is the suggested value for the integrated calculation through the day.
Zenith and azimuth divisions (sky sectors in sky map)	$18 \times 24 (\theta, \psi)$	Number of zenith and azimuth divisions to calculate diffuse radiation. An 8×8 array is sufficient; the increased resolution of the array can refine the detailed results
Diffusion model (standard overcast sky)	—	Calculates the variation of the diffuse radiation proportion as a function of change in the zenith angle
Transmittivity co-efficient (τ)	0.5–0.7	Fraction of the radiation travel across the atmosphere. Normal clear sky conditions for calculation of the monthly irradiation is 0.5
Diffusion co-efficient (τ_d)	0.2–0.4	Filtered radiation fraction by atmospheric constituents. Normal clear sky conditions is 0.3

The parameters have been considered to simulate the conditions under a clear sky suggested by Fu and Rich (1999). θ , zenith angle; ψ , azimuth angle.

Table 2. The Solar Analyst model output surface based on diffusion (τ_d) and transmissivity (τ) parameters.

ID	Output response	τ_d	τ
1	Sf-45	0.4	0.5
2	Sf-35	0.3	0.5
3	Sf-46	0.4	0.6
4	Sf-36	0.3	0.6
5	Sf-26	0.2	0.6
6	Sf-37	0.3	0.7
7	Sf-27	0.2	0.7

Values selected for the characterization of radiation in the study area (in bold).

irradiance and other meteorological variables inside the GMA for 2014.

Since the SA model shows limitations in predicting irradiation under overcast conditions (Herrick *et al.*, 1993; Dubayah and Rich, 1995; Ruiz-Arias *et al.*, 2009), the monthly irradiation from the SA response was restricted and evaluated during the dry season, when stable atmospheric conditions prevailed. The results from this season identify acceptable uncertainties arising from the predictability of the SA model.

3.4. Criteria to improve the irradiation analysis

The absence of an extensive monitoring network installed in the study area was the main limiting factor for evaluating the model's response. Therefore, the irradiation was analysed on surfaces with closely similar topography conditions at the Colomos site, which is characterized as a plain surface. The spatial boundaries to define these kinds of surfaces were based on two criteria: (1) morphological and (2) statistical standardization of the data irradiation produced by the SA model.

For the morphological criteria, it was difficult to exclude all surfaces with steep relief from the spatial analysis of irradiation, because the high relief directly influences the topographic shadow effect. However, the relief of the SRC with slope $>15^\circ$ below the elevation level of the GMA allowed 8.3% of the total study area to be discriminated. Once the surface of the SRC was subtracted from the DEM analysis, the SA model was executed over the remaining 91.7%, which was almost fully composed of plain surfaces.

Analysis of the monthly histograms of each SA irradiation surface shows that the most common irradiation values were so close to the mean value in their own matrix; these values correspond to relatively flat surfaces. The irradiation from this area was subjected to a second process of spatial delimitation. A data standardization of the irradiation matrix was performed and defined for every month. Each irradiation cell was related to the mean value and normalized by the typical deviation of the matrix. Only surfaces close to average values and within the range of $\pm 1\sigma$ were retained. The remaining data were deleted since they were outside this threshold. Afterwards, the surfaces were re-transformed to the initial values of irradiation.

3.5. Statistical analysis

During the dry season, all the SA responses were compared with Colomos data, and they had the same behaviour and trend (Figure 2). Independently of variations from the atmospheric parameters, every response has a direct relation with α changing throughout 2014 (Table 3), albeit with different magnitudes.

Table 3. Relationship between solar elevation angle (α) and date at Guadalajara latitude ($20^\circ 39' 55''$) in 2014.

Date	α	Date	α
21 January	49.5°	22 July	90.0°
20 February	58.8°	23 August	81.2°
20 March	69.6°	23 September	69.6°
20 April	81.2°	22 October	58.8°
24 May	90.0°	22 November	49.5°
21 June	87.3°	21 December	46.0°

Data taken from Solar Radiation Monitoring from the Laboratory of the University of Oregon. <http://solardat.uoregon.edu/SunChartProgram.php> (last consulted 12 July 2016).

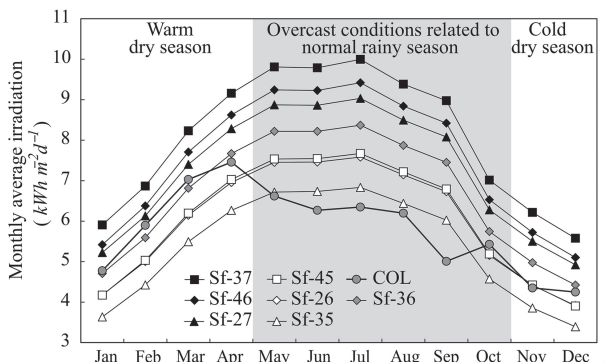


Figure 2. Behaviour of the monthly average irradiation through the annual cycle of the Guadalajara Metropolitan Area. The graphic shows the contrast between different output responses of the SA model with respect to the irradiation obtained from Colomos station (COL), in the context of seasonal change.

Because significant differences were not clearly identified, a series of statistical tests was performed to highlight the best response in order to confirm the predictive capability. From this analysis, November irradiation was excluded because it presented atypical rain conditions that interrupted the downward trend pattern of irradiation that normally takes place during the winter.

3.5.1. Correlation analysis

A linear correlation analysis was performed to explore differences between some SA responses with regard to Colomos data. A confidence level of 95% was used for all statistical tests, and the correlation degree was defined by its determination co-efficient. Through an analysis of variance (ANOVA), the significance of all relationships was observed (at least $P < 0.001$). The correlation of any response from the SA model explained approximately 95.96% of the Colomos variance. Additionally, a Durbin–Watson test on residual series between the SA model and the Colomos data confirmed the significant correlations ($d = 1.031$, $P = 0.000$).

3.5.2. Data scattering

A dispersion analysis of the data was carried out considering the differences between monthly average irradiation from the SA response and the Colomos station. The mean and standard deviation for each group was used to evaluate the relative dispersion of the responses. A benchmark (COL-100) derived from observations in Colomos was defined, and it was used to evaluate the responses of the SA model. COL-100 was obtained from

the meteorological station; this is equivalent to approximately $98.2 \pm 0.5\%$ monthly average irradiation from field observations (I_G - $100 \text{ W m}^{-2} \text{ day}^{-1}$, for every month).

3.5.3. Cluster analysis

In addition, a cluster classification was performed to identify similarities and distances, as well as to demonstrate the degree of association between the SA dataset and the Colomos station. The cluster analysis was established from the hierarchical method of agglomerates under the criterion of average linkage measurements, and using Euclidean squared distances to define the distances between members into two groups.

3.5.4. Multiple sample comparison (MSC)

The uniform behaviour trends of irradiation for any response were tested for variation. The ANOVA was used to determine differences between any of the seven SA responses and the Colomos data (comparison between groups). The null hypothesis (H_0) for this test established that there were no significant differences between the mean values of the groups. The MSC was performed based on a multiple range of tests and the Tukey-HSD method. Following the first ANOVA, two groups were excluded (Sf-35 and Sf-37). A second ANOVA was performed to validate the H_0 previously proposed ($F = 1.260$, $P = 0.308$).

3.6. SA statistical validation using daily data

Additionally, the Sf-36 was executed to evaluate irradiation on sunny days during the dry and rainy season in order to determine reference values for cloudless conditions. The periods of clear sky were identified from Colomos observations. During the dry season, the daily average irradiation was calculated systematically on five different days distributed through the month. Meanwhile, during the wet season the choice of sunny days was supported by reviewing daily records of irradiance for the season, using the following criteria: (1) high intensity and normal behaviour of radiance throughout the hours and days of each month; (2) a low percentage of humidity in the air during the day; (3) normal behaviour of the temperature without falling to dew point, and (4) the absence of precipitation events (Figure 3).

In the dry season, days with average irradiation equal to or higher than the monthly average observed at Colomos were retained for the analysis, while during the rainy season, days with the highest radiation in the month were chosen, always ensuring that the samples were roughly distributed throughout the month. There were cases when the criteria were not met. Only four samples were obtained in August and October, three in June, and September was excluded for not having enough days with a domain of clear sky.

4. Results and discussion

4.1. Characterization of the rainfall

Normal rainfall during the period 1991–2012 shows that the rainy season usually occurs between May and October, and maximum monthly accumulated rainfall occurs in July (Figure 4). Between 1991 and 2012, the total annual precipitation was 979 mm on average. Meanwhile, in 2014 it reached 855.5 mm; this is 87.4% of the normal precipitation for that period.

An important aspect is that the precipitation in 2014 was distributed in a different way. The rain was delayed a month in

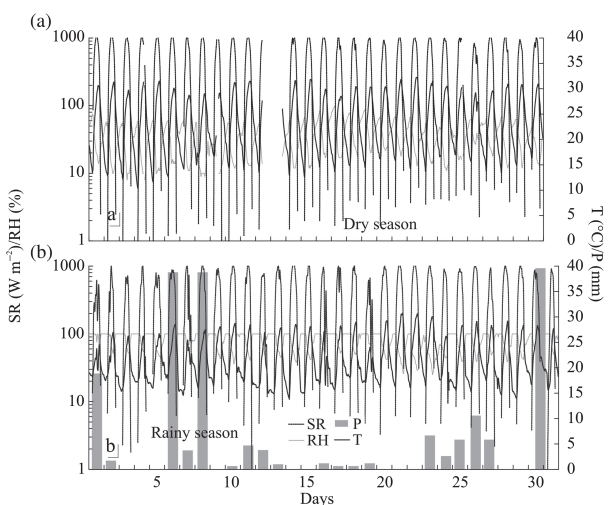


Figure 3. (a) and (b) Temporal contrast in behaviour of some meteorological variables in the Guadalajara Metropolitan Area (e.g. April and July, dry and rainy season, respectively); data obtained from the Colomos station. SR, solar irradiance; RH, relative humidity; T, temperature; P, precipitation.

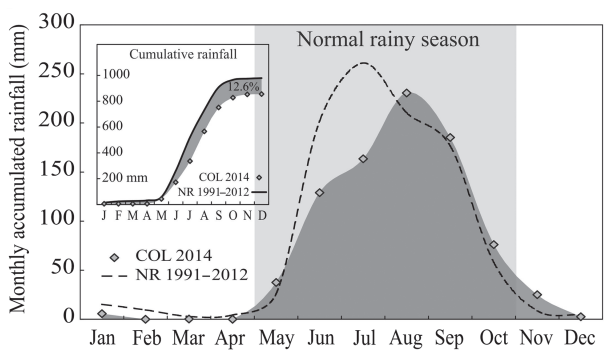


Figure 4. Annual precipitation comparison between 2014 (Colomos) and the normal behaviour of the last two decades in the Guadalajara Metropolitan Area based on the historical records from five stations of the National Meteorological Survey (Figure 1). NR, normal rainfall; COL, Colomos.

order to reach the maximum amount of monthly precipitation. In the first half of the wet season, the rainfall shows a deficit of 39% of the accumulated precipitation from the total rainfall observed in normal status. Nevertheless, this proportion was compensated by a rainfall increase in the period from August to November (Figure 4). Ultimately, there was a deficit of 12.6% in the amount of precipitation for 2014, compared with the long term average. A variance test with a confidence level of 95% indicated that there were significant differences ($F = 822.1$, $P = 0.0268$) between the 2014 rainfall and the 1991–2012 average. In addition, its correlation ($R^2 = 45.7\%$, $P = 0.210$) confirm the atypical rainfall behaviour in 2014.

4.2. Analysis of the model output responses

This study tested the efficiency of the SA response for a complete annual cycle, including both monthly and daily time scales. The model was run using the same conditions for all output responses (Table 1), considering only changes in atmospheric diffusion and transmittance conditions (Table 2). The behaviour of irradiation

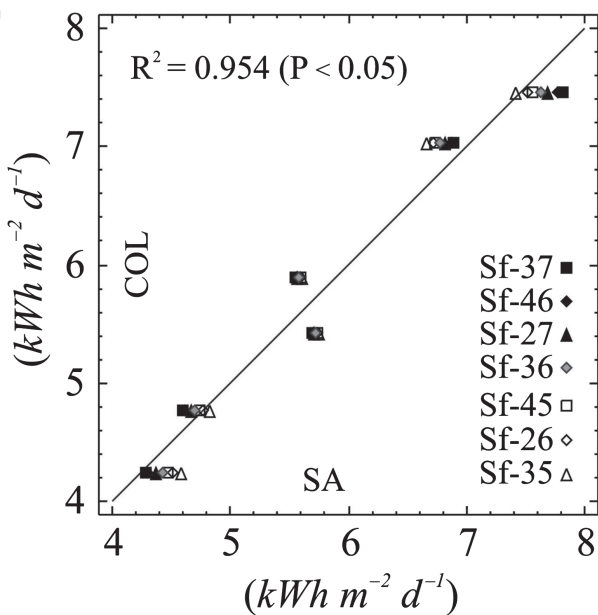


Figure 5. Analysis of correlation and variability. Model fit and correlation function of the slopes and intercepts variation between different SA output responses and the Colomos data (COL), for the dry season.

on the GMA was characterized during 2014, and a rough estimate of the proportion of irradiation attenuated throughout the rainy season was also obtained.

A direct comparison of the monthly average irradiation between Colomos and the SA model has shown that four responses (Sf-26, Sf-45, Sf-27 and Sf-36) had a good approach during the dry season (Figure 2). The ANOVA for correlation analysis between the SA responses and Colomos indicates that there is not a significant difference between slopes ($F=0.580$, $P>0.743$). This test highlights differences between the intercepts ($F=38.030$, $P<0.000$); hence, the model regression curve was redesigned assuming that only the slopes are similar to each other (Figure 5). This shows that any SA response explains approximately 95.4% of the variance observed in Colomos under different conditions of diffusion and transmittance.

Nevertheless, another set of statistical tests provides arguments for selecting one of them. The scattering analysis on proportional differences between every SA response and the Colomos data indicates that the combination of 0.3 and 0.6 for the co-efficients τ_d and τ , respectively (Sf-36), produced a response closest to the irradiation observed at Colomos throughout the dry season in 2014 (Figure 6). The cluster analysis and ANOVA for the MSC (Figure 7) showed a gradient of similarity between the SA responses and observations in Colomos. Among them, it was noted that Sf-36 explains the Colomos variations better. Therefore, Sf-36 was chosen as the most appropriate response for 2014.

On the other hand, the analysis of the daily average irradiation based on 48 days (samples) for 2014 was obtained. From these, 21 correspond to the sunny days of the rainy season. Correlation analysis indicates that Sf-36 explains approximately 96% ($P=0.000$) of the average irradiation behaviour observed at the Colomos station for sunny days during the rainy season (Figure 8), and approximately 91% ($P=0.000$) considering the full year. These results prove the good predictive power of the model, and verify that, independently of the temporal resolution,

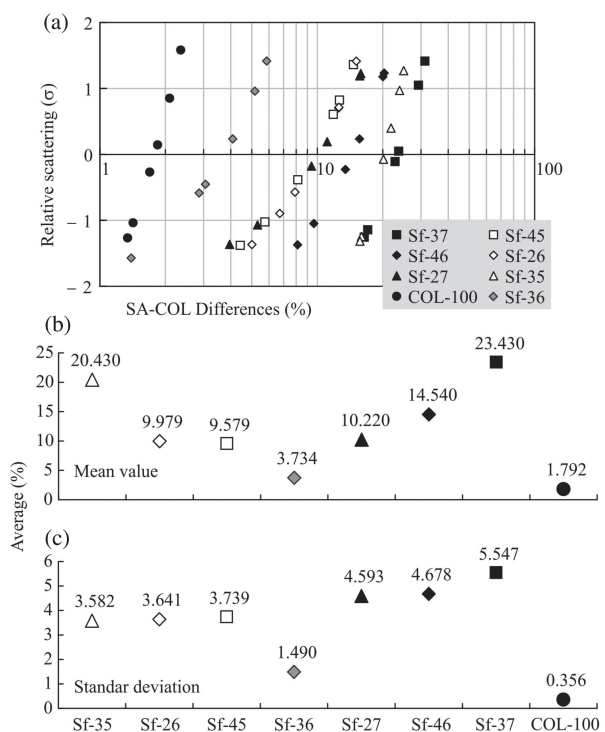


Figure 6. (a) Analysis of radiation scattering in the months of the dry season. (b), (c) Corresponding to the statistical datasets of the variables in (a).

the SA model is an excellent alternative for predicting solar irradiation.

4.3. Model approaches

The spatial analysis on the GMA was significantly improved after applying the morphological and statistical criteria. Through the subtraction of surfaces by these two criteria, an analysis of the monthly average irradiation was performed on $78.7 \pm 2.8\%$ of the total surfaces. Most of these have similar topography characteristics to the Colomos terrain. The removal of these surfaces does not affect the calculations of Sf-36. Instead, it increased the certainty of spatial analysis of the solar radiation.

The scattering from every monthly surface was reduced to a range between 14% and 28.2% compared to its mean values, i.e. $139 \text{ Wh m}^{-2} \text{ day}^{-1}$ for the winter and $71 \text{ Wh m}^{-2} \text{ day}^{-1}$ for the summer, on average (Figure 9). These approximations are very close to the monthly average irradiation observed during the dry season and the maximum daily irradiation observed in sunny days of the rainy season at the Colomos site. This means that the irradiation variability on the surface was lower in summer and greater in winter. The increase in scattering during the winter season reflects the terrain shadow effect, as well as the radiance intensity variations, which are closely related to the natural change of α throughout the annual cycle (Table 3).

The monthly average irradiation calculated with Sf-36 proved to be very efficient in predicting irradiation in the GMA. This exposed an important contrast to the irradiation from Colomos in the wet season. Its contrasts were mainly associated with overcast conditions. During the dry season, the uncertainty arising from differences between Sf-36 and Colomos was just $3.7 \pm 1.4\%$ on average. Its predictive power was not the

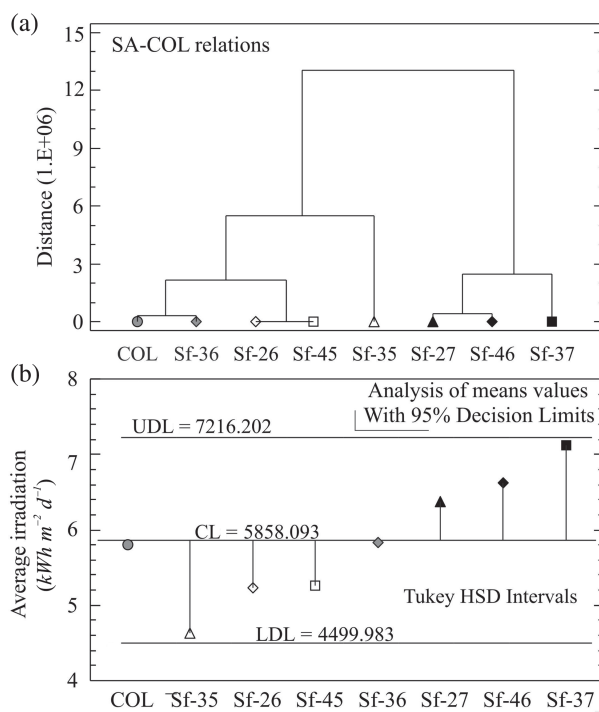


Figure 7. (a) Cluster analysis from the monthly average irradiation of the dry season. (b) Multiple comparison of samples and analysis of variance between the monthly average irradiation during the dry season, based on means analysis and decision limits (DL) (UDL, upper limit; LDL, lower limit).

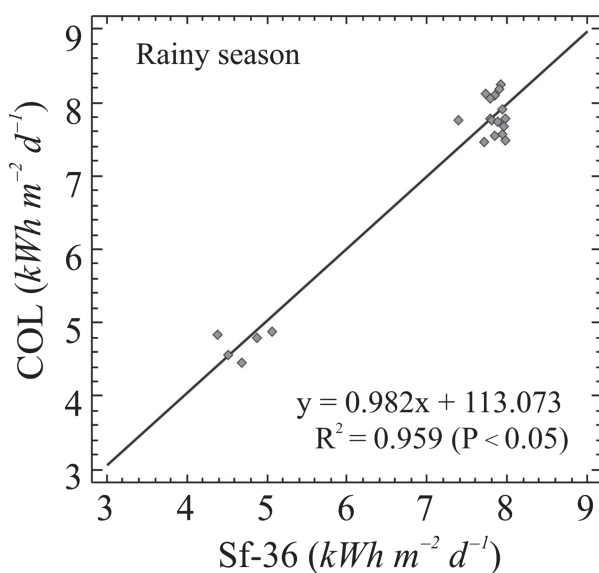


Figure 8. Correlation of the daily average radiation for sunny days in the rainy season ($n = 21$).

best in the rainy season. Meanwhile, the analysis of daily irradiation shows that there are periods with clear skies remaining for several days. These weather conditions favoured direct solar irradiation on the surface, and also showed the intensity with which it would normally reach the surface of the GMA. The correlation for irradiation during sunny days between Sf-36 and Colomos was strong; its average uncertainty values were $4.4 \pm 2.4\%$.

The annual potential irradiation given by Sf-36 was calculated as approximately $6.65 \text{ kWh m}^{-2} \text{ day}^{-1}$, with 4.69 during the winter and 8.25 for the summer season in 2014. Based on these data and field observations from the Colomos station, a significant contrast in irradiance availability was found between the dry and wet seasons. The overcast conditions related to the rainy season reduced on average $28.5 \pm 3.1\%$ of the incoming solar energy (except for September) (Figure 9). Taking into account this solar attenuating effect by overcast conditions, a new calculation of the irradiation was carried out. The annual average irradiation over the shallow relief of the GMA was estimated as $5.69 \text{ kWh m}^{-2} \text{ day}^{-1}$, with variations in the range from 5.43 to $5.80 \text{ kWh m}^{-2} \text{ day}^{-1}$ (Figure 10). These values are similar to the irradiation calculated by NASA and NREL (Table 4), which represent an excellent reference and give greater confidence to the Sf-36 results.

The results presented here have shown that the SA model depicts a highly viable alternative for studying the irradiation. Independently of the scale resolution the SA model shows a good fit, explaining at least 95% of the variability of field observations. The SA model is able to eliminate the effects of the uncertainties normally acquired when radiation is characterized with a poor spatial resolution. The results show the importance of determining the spatial contrast of the irradiation related to small areas, even when its variation is minimal.

4.4. Implications

The precipitation analysis highlights the atypical temporal behaviour of the 2014 rainfall. It must not be overlooked that this analysis was conducted in a period during which transition conditions are introduced to the warm phase of the ENSO. The cases of September and November appear to be quite atypical. In September, the irradiation was attenuated by almost 50%, a fairly high amount. This quantity does not correspond to the volume of precipitation, especially considering that August was the wettest month of the season with an attenuated irradiation percentage of 27%. September was exceptional and this appears to be related to cloud cover that was almost constant throughout the month. In November, the presence of Hurricane Vance and several cold fronts produced both a rainfall increase in the coastal region of western Mexico (CONAGUA, 2014) and major overcast conditions in the GMA. These conditions produced 15% energy attenuation in the GMA.

Based on the calculation of the potential radiation from Sf-36 and the observations made in Colomos, it is assumed that the atypical state of the precipitation during 2014 exerted a strong influence on the balance of incoming solar radiation. The 28.5% of attenuated irradiation estimated here was higher than the proportions of the irradiation which in general terms are reflected back into space by cloud cover (23%) (Kiehl and Trenberth, 1997; Fu, 2003; Trenberth *et al.*, 2009).

Locally, the correlation for irradiation on sunny days between Colomos and Sf-36 was higher during the whole year and strongest during the rainy season (Figure 8). These data do not explain significant improvements in the analysis of irradiation, but it is very likely that they reveal the effects of any physical process. The atmospheric particles and gases carried by the washing out effect caused by the rainfall of previous days could be a possible reason (Shaw, 1984; Finlayson-Pitts and Pitts, 2000).

More research related to pollutant concentrations could explain these seasonal variations. Some of them should focus on causes inherent to the random weather behaviour and atmospheric composition. Others could centre on the air thickness and

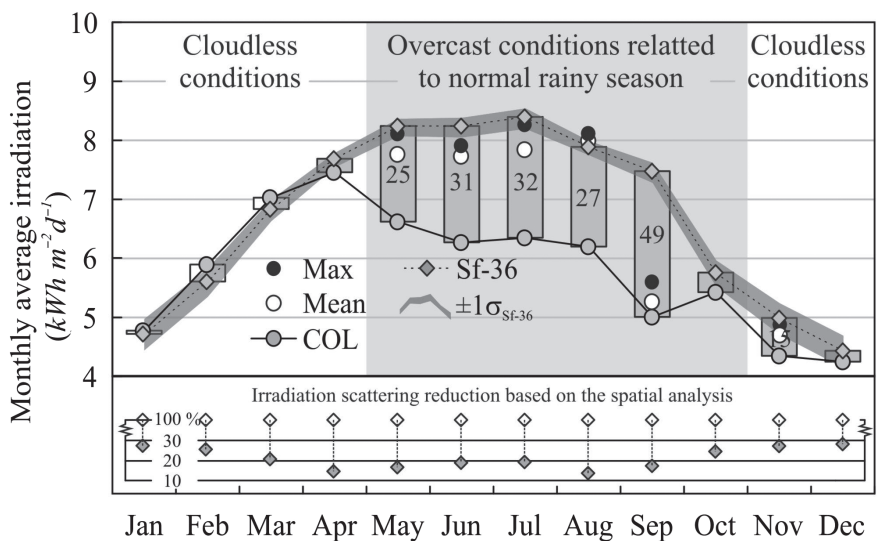


Figure 9. Behaviour of the monthly average irradiation on the Guadalajara Metropolitan Area. The figure shows the irradiation observed at the Colomos station (COL) and its contrast with the estimated irradiation by the output Sf-36 response within a $\pm 1\sigma$ threshold. Validation of Sf-36 for sunny days in the rainy season was supported by readings of maximum radiation observed in Colomos for particular days (black circles) and mean daily irradiation averaged over at least three sunny days (white circles). The grey bars show the proportion of radiation attenuated during the rainy season, determined from the potential irradiation calculated for Sf-36 and the irradiation observed in Colomos. White bars are according to an inherent underestimation of the model. The 100% of irradiation scattering is equivalent to the model typical deviation before spatial analysis.

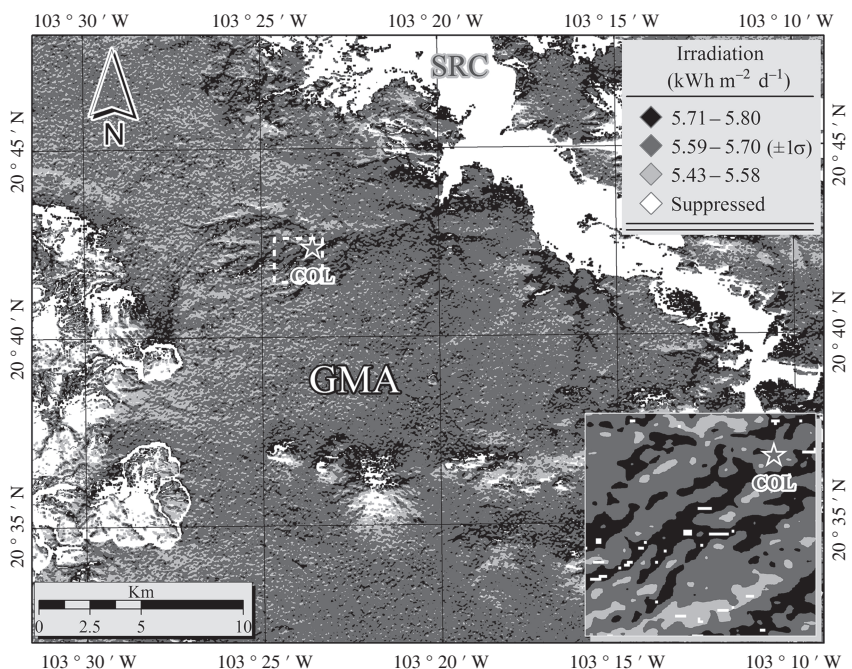


Figure 10. Map of annual average irradiation in the Guadalajara Metropolitan Area (GMA). This map represents Sf-36 potential irradiation data, fitted with the proportion of the irradiation attenuated by the overcast condition observed at the Colomos station (star position) (September was fitted based on the 28.5% estimated here). The amplitude of the irradiation values was determined on the basis of the geomorphic and statistical criteria. The surfaces suppressed by these criteria correspond to 21% of the total area (white). The irradiation class boundaries were defined through their own scattering data, considering $\pm 1\sigma$ around the mean values.

turbidity, as well as its relationship to acute pollution events (e.g. forest fires in adjacent areas, inversions, specific atmospheric conditions at weekends or peak hours). These findings could help to identify the source of these deviations and, where possible, to reduce their impact on the model uncertainty by identifying the proportions in the τ_d and τ co-efficients.

5. Conclusions

The Solar Analyst (SA) model by means of Sf-36 proved to be very efficient in predicting irradiation. The uncertainty arising from differences between Sf-36 and Colomos was just $3.7 \pm 1.4\%$ on average during the dry season, and $4.4 \pm 2.4\%$ over the rainy season.

Table 4. Annual average irradiation on the Guadalajara Metropolitan Area.

Sources	January	February	March	April	May	June	July	August	September	October	November	December	Annual
COL	4.8	5.9	7.0	7.5	6.6	6.3	6.3	6.2	5.0	5.4	4.3	4.2	5.8
NASA ^a	4.8	5.8	6.9	7.2	7.2	6.2	5.7	5.6	5.2	5.4	5.2	4.6	5.8
NREL ^a	4.7	5.4	6.6	7.0	7.3	6.2	5.4	5.4	5.3	5.3	4.9	4.3	5.7
Sf-36 ^b	4.7	5.6	6.8	7.7	6.2	5.7	5.7	5.8	5.3	5.7	4.2	4.4	5.7

COL, Colomos data.

^aData obtained from <http://maps.nrel.gov/swera> (last consulted 12 July 2016).

^bMonthly average irradiation during 2014's rainy season was corrected by the differences obtained with regard to Colomos (dark grey cells). The irradiation in September was corrected with the mean value estimated of 28.5%.

Regarding the rainfall climatology from *ca* 20 years ago, the rainfall distribution in 2014 had significant contrasts. Both the temporary delay in the wet season and the September to December rainfall trends could be early signs of the El Niño-Southern Oscillation transitional state from the neutral to the warm phase, which was formally recognized in September 2014 by the Climate Prediction Center. In the light of these results, it can be concluded that 28.5% of the incoming solar irradiation was attenuated in this year. Taking into account the general energy balance model, this is a proportion higher than the irradiation reflected back into space by cloud cover. This high proportion of energy attenuated during 2014 may be a local effect produced by overcast conditions associated with the El Niño-Southern Oscillation.

This study shows the proportion of solar energy attenuated, which was calculated under atypical weather conditions. Extrapolation of this type of analysis to other yearly cycles will be necessary in order to identify the normal proportions of solar radiation attenuated during the wet season on the Guadalajara Metropolitan Area. Furthermore, studies into the precipitation variability will be needed to identify the effects of low-frequency phenomena and their effects on the availability of radiation at the Earth's surface.

Acknowledgements

The authors would like to thank the reviewers for their valuable comments. They also thank the National Water Commission and the National Meteorological Survey in Mexico for the meteorological data, as well as the United States Geological Survey for the SRTM data. This work was supported by the National Council of Science and Technology in Mexico (log key: CB-2012/183444).

References

- Almanza R, Lopez S. 1978. Total solar radiation in Mexico using sunshine hours and meteorological data. *Sol. Energy* **21**: 441–448.
- Atwater MA, Ball JT. 1978. Intraregional variations of solar radiation in the eastern United States. *J. Appl. Meteorol.* **17**(8): 1116–1125.
- Atwater MA, Brown PS Jr. 1974. Numerical computations of the latitudinal variation of solar radiation for an atmosphere of varying opacity. *J. Appl. Meteorol.* **13**(2): 289–297.
- Behrang MA, Assareh E, Ghanbarzadeh A, Noghrehabadi AR. 2010. The potential of different artificial neural network (ANN) techniques in daily global solar radiation modeling based on meteorological data. *Sol. Energy* **84**(8): 1468–1480.
- Bosch JL, Lopez G, Battles FJ. 2008. Daily solar irradiation estimation over a mountainous area using artificial neural networks. *Renew. Energy* **33**(7): 1622–1628.
- Burrough PA. 1986. *Principles of Geographical Information Systems for Land Resources Assessment*. Oxford University Press: New York, NY; 194 p.
- Campos-Aranda DF. 1992. *Procesos del ciclo hidrológico*. Facultad de Ingeniería de la Universidad de San Luis Potosí: México.
- CONAGUA. 2014. Reporte del clima en México, Gerencia de Meteorología y Climatología del Servicio Meteorológico Nacional. Año 4, Núm. 11, México, DF, 26 p.
- Davydova B, V, Skiba YN. 1999. Climate of Guadalajara City (México), its variation and change within latest 120 years. *World Res. Rev.* **11**(2): 258–270.
- Djurđević DZ. 2011. Perspectives and assessments of solar PV power engineering in the Republic of Serbia. *Renew. Sustainable Energy Rev.* **15**(5): 2431–2446.
- Dubayah R, Rich PM. 1995. Topographic solar analysts for GIS. *Int. J. Geogr. Info. Syst.* **9**(4): 405–419.
- Elias T, Haefelin M, Drobinski P, Gomes L, Rangognio J, Bergot T, et al. 2009. Particulate contribution to extinction of visible radiation: pollution, haze, and fog. *Atmos. Res.* **92**(4): 443–454.
- Estrada-Cajigal V, Almanza R. 2005. *Irradiación global, directa y difusa, en superficies horizontales e inclinadas, así como irradiación directa normal, en la República Mexicana*, Series del Instituto de Ingeniería, Universidad Nacional Autónoma de México, México, D.F. Vol. **646**.
- Finlayson-Pitts BJ, Pitts JN Jr. 2000. *Chemistry of the Upper and Lower Atmosphere: Theory, Experiments, and Applications*. Academic Press: San Diego, CA.
- Fu Q. 2003. Solar radiation. In *Encyclopedia of Atmospheric Sciences*, Holton J, Pyle J, Curry J (eds). Academic Press: Amsterdam; 1859–1863.
- Fu P, Rich PM. 1999. Design and implementation of the solar analyst: an ArcView extension for modeling solar radiation at landscape scales. *Proceedings of the 19th Annual ESRI User Conference*, July 1999, San Diego, CA; 1–33.
- Fu P, Rich PM. 2002. A geometric solar radiation model with applications in agriculture and forestry. *Comput. Electron. Agric.* **37**(1): 25–35.
- Galindo I, Castro S, Valdés M. 1991. Satellite derived solar irradiance over Mexico. *Atmósfera* **4**(3): 189–200.
- García E. 1988. *Modificaciones al sistema de clasificación climática de Köppen*. Instituto de Geografía, Universidad Nacional Autónoma de México: México.
- Garnier BJ, Ohmura A. 1968. A method of calculating the direct short-wave radiation income of slopes. *J. Appl. Meteorol.* **7**(5): 796–800.
- Gastli A, Charabi Y. 2010. Solar electricity prospects in Oman using GIS-based solar radiation maps. *Renew. Sustainable Energy Rev.* **14**(2): 790–797.
- Hetrick WA, Rich PM, Barnes FJ, Weiss SB. 1993. GIS-based solar radiation flux models. American Society for Photogrammetry and Remote Sensing Technical Papers, 3. Photogrammetry and Modeling; 132–143.
- Hofierka J, Suri M. 2002. The solar analyst for open source GIS: implementation and applications. *Proceedings of the Open Source GIS-GRASS Users Conference*, 11–13 September 2002, Trento, Italy; 1–19.
- Iqbal M. 1983. *An Introduction to Solar Radiation*. Academic Press: Ontario, Canada; 390 p.
- Janke JR. 2010. Multicriteria GIS modeling of wind and solar farms in Colorado. *Renew. Energy* **35**(10): 2228–2234.
- Jauregui E, Luyando E. 1999. Global radiation attenuation by air pollution and its effects on the thermal climate in Mexico City. *Int. J. Climatol.* **19**(6): 683–694.
- Kiehl JT, Trenberth KE. 1997. Earth's annual global mean energy budget. *Bull. Am. Meteorol. Soc.* **78**(2): 197–208.
- Koca A, Oztop HF, Varol Y, Koca GO. 2011. Estimation of solar radiation using artificial neural networks with different input parameters for Mediterranean region of Anatolia in Turkey. *Expert Syst. Appl.* **38**(7): 8756–8762.

- Kumar L, Skidmore AK, Knowles E. 1997. Modelling topographic variation in solar radiation in a GIS environment. *Int. J. Geogr. Info. Sci.* **11**(5): 475–497.
- Lee M, Koo C, Hong T, Park HS. 2014. Framework for the mapping of the monthly average daily solar radiation using an advanced case-based reasoning and a geostatistical technique. *Environ. Sci. Technol.* **48**(8): 4604–4612.
- Lewis MR, Carr ME, Feldman GC, Esaias W, McClain C. 1990. Influence of penetrating solar radiation on the heat budget of the equatorial Pacific Ocean. *Nature* **347**(6293): 543–545.
- Li DH, Wong SL. 2007. Daylighting and energy implications due to shading effects from nearby buildings. *Appl. Energy* **84**(12): 1199–1209.
- Limon-Sánchez MT, Carbajal-Romero P, Hernández-Mena L, Saldarriaga-Noreña H, López-López A, Cosío-Ramírez R, et al. 2011. Black carbon in PM 2.5, data from two urban sites in Guadalajara, Mexico during 2008. *Atmos. Pollut. Res.* **2**(3): 358–365.
- Linares-Rodríguez A, Ruiz-Arias JA, Pozo-Vázquez D, Tovar-Pescador J. 2011. Generation of synthetic daily global solar radiation data based on ERA-Interim reanalysis and artificial neural networks. *Energy* **36**(8): 5356–5365.
- Mckenney DW, Mackey BG, Zavitz BL. 1999. Calibration and sensitivity analysis of a spatially-distributed solar analyst. *Int. J. Geogr. Info. Sci.* **13**(1): 49–65.
- Miklánek P. 1993. The estimation of energy income in grid points over the basin using simple digital elevation model. *Ann. Geophys.* **11**(Suppl. 2): 296.
- Monteith J, Unsworth M. 2013. *Principles of Environmental Physics: Plants, Animals, and the Atmosphere*. Academic Press: Oxford, UK.
- Noia M, Ratto CF, Festa R. 1993a. Solar irradiance estimation from geostationary satellite data: I. Statistical models. *Sol. Energy* **51**(6): 449–456.
- Noia M, Ratto CF, Festa R. 1993b. Solar irradiance estimation from geostationary satellite data: II. Physical models. *Sol. Energy* **51**(6): 457–465.
- Perez R, Ineichen P, Moore K, Kmiecik M, Chain C, George R, et al. 2002. A new operational satellite-to-irradiance model. *Sol. Energy* **73**(5): 307–317.
- Perez R, Schlemmer J, Renne D, Cowlin S, George R, Bandyopadhyay B. 2009. Validation of the SUNY satellite model in a meteosat environment. *Proceedings ASES Annual Conference, Buffalo*, January 2009, New York, NY.
- Pinker RT, Laszlo I. 1992. Modeling surface solar irradiance for satellite applications on a global scale. *J. Appl. Meteorol.* **31**: 194–211.
- Pons X. 2002. MiraMon. Geographical information system and remote sensing software. Version 4.4.
- Pons X, Ninyerola M. 2008. Mapping a topographic global solar analyst implemented in a GIS and refined with ground data. *Int. J. Climatol.* **28**(13): 1821–1834.
- Ramírez-Sánchez HU, Andrade-García MD, Bejarano R, García-Guadalupe ME, Wallo-Vázquez A, Pompa-Toledano AC, et al. 2009. The spatial-temporal distribution of the atmospheric polluting agents during the period 2000–2005 in the urban area of Guadalajara, Jalisco, Mexico. *J. Hazard. Mater.* **165**(1): 1128–1141.
- Reddy SJ. 1971. An empirical method for the estimation of total solar radiation. *Sol. Energy* **13**(2): 289–290.
- Reddy SJ. 1974. An empirical method for estimating sunshine from total cloud amount. *Sol. Energy* **15**(4): 281–285.
- Remund J, Wald L, Lefèvre M, Ranchin T, Page J. 2003. Worldwide Linke turbidity information. *ISES Solar World Congress 2003*, June 2003, International Solar Energy Society (ISES), Vol. 400, 13.
- Revfeim KJA. 1978. A simple procedure for estimating global daily radiation on any surface. *J. Appl. Meteorol.* **17**(8): 1126–1131.
- Rich PM, Clark DB, Clark DA, Oberbauer SF. 1993. Long-term study of solar radiation regimes in a tropical wet forest using quantum sensors and hemispherical photography. *Agric. For. Meteorol.* **65**(1): 107–127.
- Rich PM, Hetrick WA, Saving SC, Dubayah R. 1994. Using viewshed models to calculate intercepted solar radiation: applications in ecology. American Society for Photogrammetry and Remote Sensing Technical Papers; 524–529.
- Rich PM, Weiss SB, Debinski DA, McLaughlin JF. 1992. Physiographic inventory of a tropical reserve. *Proceedings of the Twelfth Annual ESRI User Conference*, 8–12 June 1992, Plam Springs, CA; 197–208.
- Robinson D. 2006. Urban morphology and indicators of radiation availability. *Sol. Energy* **80**(12): 1643–1648.
- Robinson D, Stone A. 2004. Solar radiation modelling in the urban context. *Sol. Energy* **77**(3): 295–309.
- Ruiz-Arias JA, Tovar-Pescador J, Pozo-Vázquez D, Alsamamra H. 2009. A comparative analysis of DEM-based models to estimate the solar radiation in mountainous terrain. *Int. J. Geogr. Info. Sci.* **23**(8): 1049–1076.
- Rumbayan M, Abudureymu A, Nagasaka K. 2012. Mapping of solar energy potential in Indonesia using artificial neural network and geographical information system. *Renew. Sustainable Energy Rev.* **16**(3): 1437–1449.
- Senkal O. 2010. Modeling of solar radiation using remote sensing and artificial neural network in Turkey. *Energy* **35**(12): 4795–4801.
- Shaw RW. 1984. The atmosphere as delivery vehicle and reaction chamber for acid precipitation, In *Meteorological Aspects of Acid Rain*, Bhumralker CM (ed), *Acid Precipitation Series*, Teasley JL (ed), Vol. 1. Stoneham, MA; 33–55.
- Sorensen B. 2001. GIS management of solar resource data. *Solar energy materials and solar cells* **67**(1): 503–509.
- Swift LW. 1976. Algorithm for solar radiation on mountain slopes. *Water Resour. Res.* **12**(1): 108–112.
- Swift LW, Knoerr KR. 1973. Estimating solar radiation on mountain slopes. *Agric. Meteorol.* **12**: 329–336.
- Tarpley JD. 1979. Estimating incident solar radiation at the surface from geostationary satellite data. *J. Appl. Meteorol.* **18**(9): 1172–1181.
- Tereshchenko IE, Filonov AE. 1997. A cerca de las causas de las elevadas concentraciones de ozono en la atmósfera de la Zona Metropolitana de Guadalajara, en octubre de 1996. *GEOS* **17**: 54–59.
- Tovar-Pescador J, Pozo-Vázquez D, Ruiz-Arias JA, Battles J, López G, Bosch JL. 2006. On the use of the digital elevation model to estimate the solar radiation in areas of complex topography. *Meteorol. Appl.* **13**(3): 279–287.
- Trenberth KE, Fasullo JT, Kiehl J. 2009. Earth's global energy budget. *Bull. Am. Meteorol. Soc.* **90**(3): 311–323.
- Valdés-Barrón M, Riveros-Rosas D, Arancibia-Bulnes CA, Bonifaz R. 2014. The solar resource assessment in Mexico: state of the art. *Energy Procedia* **57**: 1299–1308.
- Williams LD, Barry RG, Andrews JT. 1972. Application of computed global radiation for areas of high relief. *J. Appl. Meteorol.* **11**(3): 526–533.
- Wilson JP, Gallant JC. 2000. Secondary topographic attributes. In *Terrain Analysis: Principles and Applications*, Wilson JP, Gallant JC (eds). John Wiley and Sons: New York, NY; 87–131.
- Yu B, Liu H, Wu J, Lin WM. 2009. Investigating impacts of urban morphology on spatio-temporal variations of solar radiation with airborne LIDAR data and a solar flux model: a case study of downtown Houston. *Int. J. Remote Sens.* **30**(17): 4359–4385.
- Zakšek K, Podobnikar T, Oštir K. 2005. Solar radiation modelling. *Comput. Geosci.* **31**(2): 233–240.

WEBSITES

- <http://earthexplorer.usgs.gov/>
<http://maps.nrel.gov/swera/>
<http://smn.cna.gob.mx/es/emas/>
<http://solardat.uoregon.edu/>
- Last consulted: 12 July 2016 (For all sites)